

Material Failure Assessment of Leakage in a Low Alloy Steel Choke Body



J. Alias and N. A. Alang

Abstract This paper highlighted the material failure of the low nickel–chromium–molybdenum steel choke body by visual observation, microstructure characterization, chemical composition, and hardness analysis. A choke body failed due to leakage at the choke body after 11 years in service. A combination of fluid flow condition and electrochemical reaction of the choke body in the non-associated gas (NAG) containing CO₂ environment induces localised corrosion such as erosion and preferential weld corrosion (PWC). The severe corrosion penetration along the weld bead adjacent to the eroded region was observed as the primary cause of choke body leakage. The evidence of less chromium composition at the weldment region due to carbide coarsening could contribute to the decrease in corrosion resistance and induce localized corrosion of the weldment leading to PWC. To prevent the recurrence of failure, it is recommended that the material of the weldment should be of high corrosion resistance, which can be achieved by microstructure modification and avoidance of galvanic reaction between the weldment and other regions. Careful consideration of the fluid flow condition is also required as it may exacerbate the PWC.

Keywords Choke valve · Low alloy steel · Erosion corrosion · Preferential weld corrosion · Microstructure

1 Introduction

Diverse grades of steel and stainless steels are used for the majority of process devices, for example, pipe, tube, fitting devices, valves and chokes used in the oil

J. Alias (✉)

Department of Mechanical Engineering, College of Engineering, Universiti Malaysia Pahang, 26300 Gambang, Kuantan, Pahang, Malaysia
e-mail: juliawati@ump.edu.my

N. A. Alang

Faculty of Mechanical and Automotive Engineering Technology, Universiti Malaysia Pahang, 26600 Pekan, Pahang, Malaysia

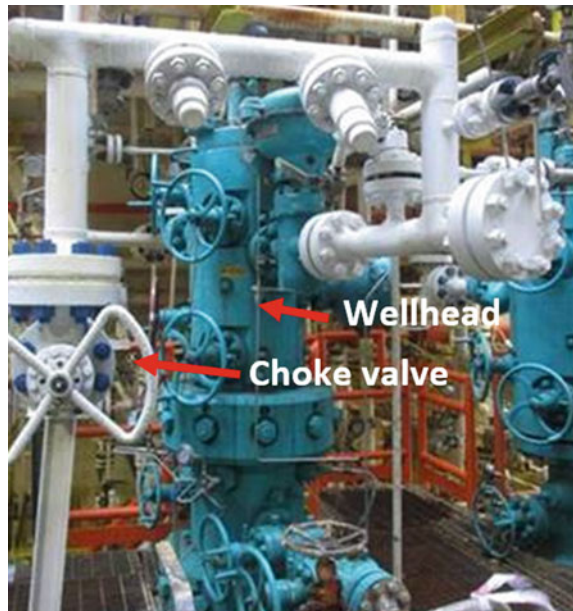
and gas sector due to economic and good characteristics reasons [1–3]. Plain carbon steels such as API 5L, ASTM A106 are the most commonly used alloys for these applications. However, they are unable to meet the needs of the modern oil industry for greater wear and corrosion resistant. The use of low alloy steel, which containing up to 1 wt.% of Cr, is a type of steel developed specifically for the use in CO₂ environments for high strength and good hardenability [4, 5].

A choke valve is a mechanical device that induces restriction in a flow line, causing either a pressure drops or a reduction in the rate of flow. In the oil and gas industry, choke valves are normally located on top of each well, as depicted in Fig. 1 [6]. The choke valves are used to control the pressure on several wells into a common manifold. Chokes used in oil and gas wells are classified into two types depending upon the operation mode, either be adjustable or positive. Adjustable chokes are flexible in that they allow the fluid flow and pressure to be adjusted in accordance with production requirements. Positive chokes do not provide that flexibility; however, they are more resistant to damage by abrasion or erosion.

A mixture of the fluids, inhibitors and output hydrocarbons, including oil, gas, water, sand, H₂S and even CO₂, is regulated by choking valves. During operation, chokes are vulnerable to a variety of types of damage and localised corrosion, including erosion, wear, cavitation, weld corrosion, stress corrosion cracking, and corrosion fatigue [6–9].

Carbon dioxide, CO₂-corrosion is the most prominent failure cause on the steel equipment due to material's synergistic impact during operation in CO₂-containing medium. As a result, it is important to conduct a thorough investigation to determine

Fig. 1 Flow line consists of wellhead and choke valve



the root cause of the failure in order to avoid it in the future. The influence of dissolved carbon dioxide on the increase of the carbon steel corrosion rate has been studied by [10]. Carbon dioxide (CO_2) is generally non-corrosive in the gaseous state. However, hydration has taken place and a more reactionary chemical species, carbonic acid (H_2CO_3), has been produced in the presence of water and hydrogen. The reaction is then accompanied by a dissociation reaction, which leads to acidic, corrosive solution [11–13] in order to form bicarbonate (HCO_3^-), carbonate (CO_3^{2-}), and hydrogen (H^+) ions. The formation and chemical inhibition of iron carbonate, FeCO_3 and iron sulphide and FeS help minimise carbon steel corrosion rates. However, the iron carbonate/sulphide scale or protective inhibitor layer may be affected by the small amount of sand or debris and therefore create a synergistic erosion-corrosion effect.

As a result, internal corrosion risk assessment and corrosion inhibition must be considered to ensure technical integrity over the equipment's lifetime. In the last two decades, however, the results have questioned the explicitly labeled concepts regarding these process mechanisms [14–19].

This paper focuses on the damage analysis involved in the leaked steel choke body in order to determine the mechanisms and cause of the corrosion.

2 Method and Materials

According to the documentation and inspection histories, the choke body was constructed of two different sections and joined by a fusion welding process. The first section consists of the valve body until the choke seat, while another section is from the downstream of the choke seat until the outlet. The design life was 25 years. The inlet and outlet diameters of the valve were 3" and 4" outer diameter (OD), respectively. The operating temperature and pressure of the steam water were in the range of 6.6–120 °C and 800 psi, respectively. The working flow rate was measured at 14 mmscf. The medium of the choke body consisted of non-associated gas (NAG) with 15% CO_2 and less than 2 ppm H_2S content. Water content was measured approximately 1110 bbl per day.

The first leakage was started at the weldment after about 11 years in service. It was then repaired by insulating with Belzona metal repair. After 7 months, the leakage was leaked at the choke body that caused well shut. Accordingly, the choke was replaced by a second choke of the same design and material of construction from another flowline, which then failed again after less than 12 months service. Schematic diagram of leakage locations at the weldment and the surrounding environment of the choke valve is provided in Fig. 2. The choke body was cut carefully and split to half to observe the internal condition. An oxy-acetylene torch was used to separate both the flange units and followed by a milling process to cut the choke body. Manual cutting machine was then used to prepare small samples for microstructure characterization and hardness measurement.

Sample for microstructure characterization was mounted, mechanical ground from 240 grit abrasive paper to 1200 grit, and polished with diamond slurry. The

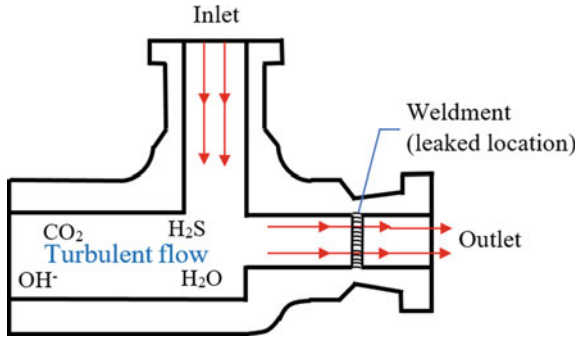


Fig. 2 Schematic diagram of leaked locations at weldment and the surrounding environment of the choke body

sample was finally etched with 2% Nital solution for 3 s. The microstructure of the outlet, inlet and weldment regions was observed using optical microscopy. A similar sample was applied for Vickers microhardness for 15 indentations at three measurement regions for accuracy and reproducibility. The Vickers method was performed in compliance with ASTM E384-17. The applied load for the hardness test was 100 gf.

Positive material identification (PMI) was conducted to the body material of three regions; inlet, outlet and weldment, by using optical emission spectroscopy (OES). The leaked region was observed further by using a low magnification stereo microscope. The analysis of the corrosion product was performed by FEI scanning electron microscope (SEM) and Bruker D8 Advance X-Ray Diffractometer (XRD). The pattern was recorded from 7° to 100° 2θ using cobalt $\text{K}\alpha$ radiation for phase identification.

3 Results and Discussion

3.1 Visual Observation

Figure 3 depicts the as-received split half of the leaked choke body. The sample obtained by sectioning around the weldment adjacent to the leaked region and then metallographic preparation is shown in the inset image. The unit's exterior surface is in excellent condition, with no visible signs of mechanical damage, dent, or gauging. There are no signs of rust, and the coating is in good condition. The inner surface revealed significant metal loss, especially downstream of the choke seat, severe corrosion penetration at the weldment, an erosion pattern, and a few cavitation downstream of the outlet.

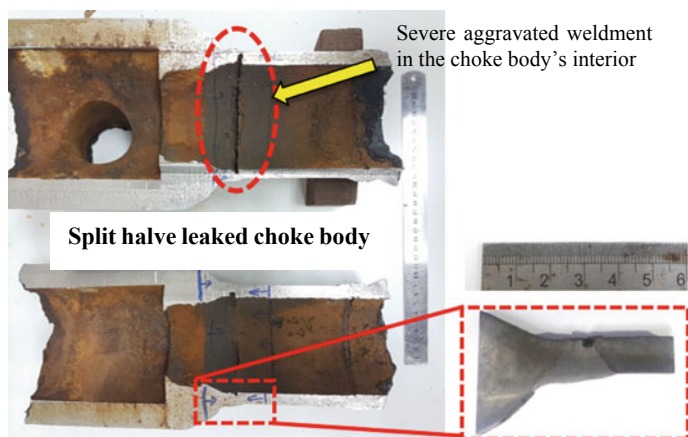


Fig. 3 Overview of split halve of the choke valve. The inset image displays the sample obtained by sectioning around the weldment adjacent to the leaked region and further proceeded for metallographic preparation

3.2 Chemical Composition

The chemical composition of the choke body material is listed in Table 1. The composition was conformed to the specified ASTM standard, A487 Grade 4 and 9 for standard specification for steel castings suitable for pressure service [20]. The compositions of ASTM A487 Grade 4 and 9 were included in Table 2. Both materials' alloying content is nearly in the nominal range for the referred composition, but lower Cr content was measured at the weldment area. The body material is cast steel that has been quenched and tempered as part of the heat treatment for product fabrication, according to the ASTM A487 standard specification for steel castings suitable for pressure operation. Both alloys have tempering temperatures ranging from 595 to 675 °C.

The inlet compositions are referred to the composition of ASTM A487 Grade 4, while the outlet compositions are referred to ASTM A487 Grade 9 [20].

Table 1 Measured chemical composition of choke valve's material including inlet, outlet and weldment region

Area	Element composition (wt.%)								
	C	Si	Mn	P	Mo	S	Cr	Ni	Fe
Inlet	0.157	0.228	0.777	0.004	0.183	0.007	0.50	0.504	Bal
Outlet	0.295	0.241	0.556	0.007	0.235	0.004	1.11	0.182	Bal
Weldment	0.107	0.293	1.920	0.009	0.377	0.004	0.093	0.395	Bal

Table 2 Nominal referred composition of ASTM A487 Grade 4 and ASTM A487 Grade 9

Limits	Nominal composition (wt.%)										
	C	Si	Mn	P	Mo	S	Cr	Ni	Fe		
ASTM A487 Grade 4 (inlet)	0.30 max	0.80 max	1.00 max	0.04 max	0.15-0.30	0.045 max	0.40-0.80	0.40-0.80	Bal		
ASTM A487 Grade 9 (outlet)	0.05-0.33	0.80 max	0.60-1.00	0.04 max	0.15-0.30	0.045 max	0.75-1.10	N/A	Bal		

3.3 Microstructural Characterization

Figure 4a shows the overview of the sectioned sample for microstructure observation at outlet (A), inlet (C) and weldment (B) regions. Figure 4b and d shows the microstructures of both inlet and outlet consist of a fully tempered martensite structure. Finer size of tempered martensite at the outlet was observed than the inlet region, as the outlet is made of grade 4 steel casting, while the inlet is Grade 9 steel casting, which conformed by the composition analysis. The welded region consisted of a variation of microstructure (Fig. 4c), including grain boundary ferrite (GBF) and also evident of coarse martensite. The transformation of microstructures and properties during tempering is generally dependent on the primary microstructure. Precipitation of cementite, Fe_3C , occurred during tempering from the martensitic process due to the reaction of iron with carbon in the solid state, accompanied by the formation of rich-carbide-(Mo,Cr) precipitates and carbide coarsening [21, 22]. As a result, the composition of C and Cr at the weldment, as shown in Table 1, is reduced due to carbon segregation to form Cr-carbide precipitates.

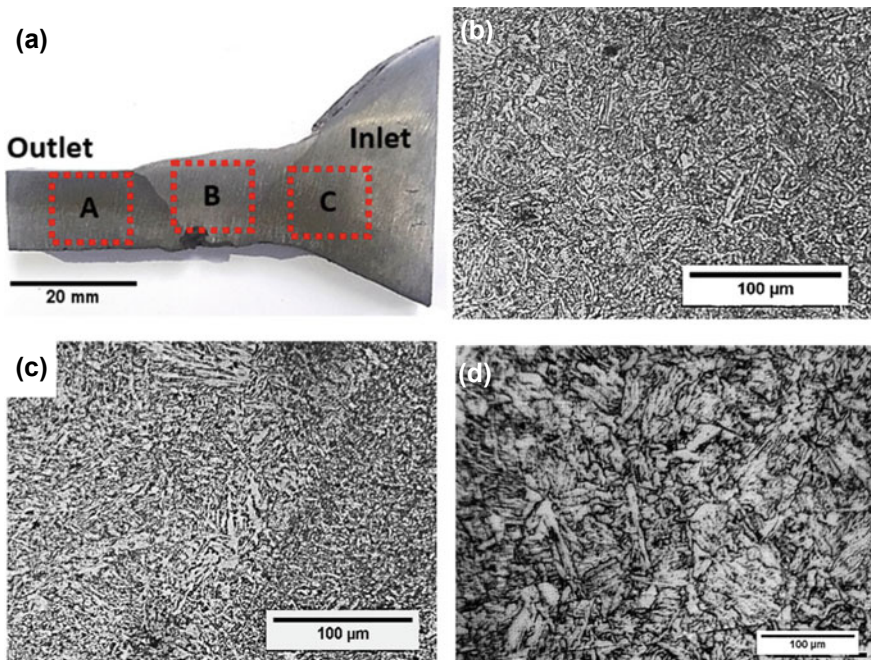


Fig. 4 a Overview of sectioned sample for microstructure observation at outlet (A), inlet (C) and weldment (B) regions; b tempered martensite microstructure observed at outlet (A); c tempered martensite and GBF microstructure at weldment (B); and d tempered martensite microstructure at inlet (C). Take note that the micrograph of inlet region (C) has been enlarged with magnification of 20×

3.4 Hardness Profile

Hardness test was conducted for the choke body near to the welded region by using Vickers microhardness. The hardness value is influenced by the heat input level, chemical composition and microstructure development during welding. The profile of hardness is aimed to reveal any effect of hardness and microstructural dependence on PWC. Three (3) measurements of 25 indentation points were plotted across the region of the weldment, with a distance of 0.5 mm between an indentation. Figure 5 displays the hardness profile across the distance. The average hardness value as shown in Table 3, indicated the hardness value at weldment-fusion boundary of

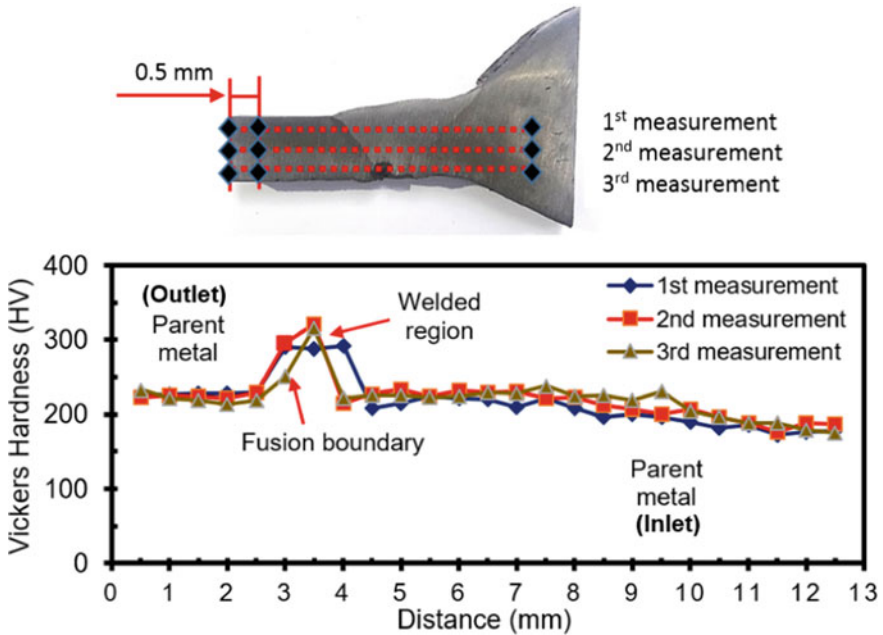


Fig. 5 Indentation points during hardness test and hardness profile across the distance (mm) of parent metal (outlet and inlet) and welded region

Table 3 Average Vickers microhardness (HV) of the welded region and parent metal

Measurement	Fusion boundary-welded region (HV)	Outlet parent metal (HV)	Inlet parent metal (HV)
1	290	228	200
2	309	224	211
3	283	221	213
Average	294	224	208
Standard Dev.	13.5	3.5	7

294 HV based on the three hardness measurements. Both outlet and inlet materials indicated a hardness value of 224 HV and 208 HV, respectively. The hardness level of weldment and the other region is considered more than those recommended based on NACE standard practice, SP0472 in H₂S-containing environment which ruled out the maximum allowable weld deposit hardness of 210 HV and 248 HV for heat-affected zone (HAZ) to prevent environmental crack occurrence [23]. By taking into account on the structure of body-centered tetragonal (BCT) of the alloy, the carbon trapping in the alloy following the carbide precipitation, induced strain field in the cell and restricted the dislocation movement. The precipitation of carbide in (Cr, Mo) will then begin, and thus, the precipitation strengthening becomes effective [24–26]. Furthermore, as the weldment having a mixture of martensite and GBF, the carbide coarsening became inevitable and increases the strength and hardness. Coarser carbide determines the increase of hardness value. The use of Hollomon-Jaffe parameter is usually referred to dictate the changes in the hardness of steel during tempering [27, 28].

3.5 Damage Analysis

The inspection of point of leakage is applied by using dye penetrant test to the choke body. A pin-hole was identified as marked by yellow arrows shown in Fig. 6a. From the inspection, two pinholes in the size of less than 10 mm were detected at the weldment region. Observing to the internal body (Fig. 6b), pink colorant of dye penetrant marked the exact location of pinhole, depicted by yellow arrow. The pinhole

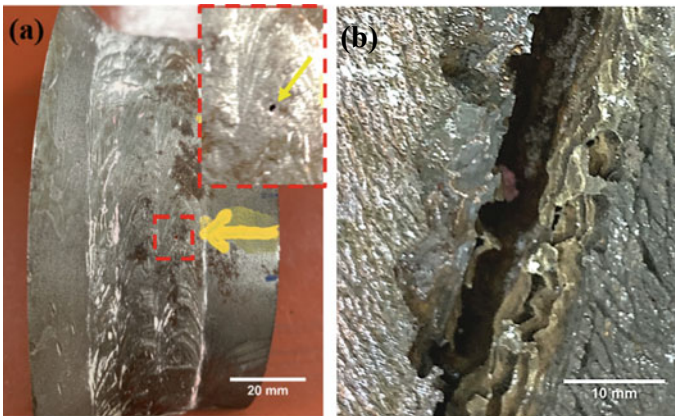


Fig. 6 Image of pinhole located at weldment **a** observing from the outer choke body. The inset image displays the enlarged image of the pinhole in red dash box, and **b** pink colorant from dye penetrant test indicated the location of pinhole, observed from inner choke body

is located at the corroded region which was deeply aggravated than the surrounding regions.

3.6 Localized Damage by Erosion Corrosion

Figure 7 displays the micrograph of the corroded choke body adjacent to the severely degraded weldment. Erosion corrosion is obviously figured based on the flow pattern direction. In this case, the flow pattern has obviously followed the direction to the outlet suggesting the occurrence of vortices of flow. Under the operational temperature (6.6–120 °C) and pressure of about 800 psi, at the corroded area, the flow-accelerated corrosion or erosion corrosion is possible.

According to Barker et al. [16], corrosion failures occur in regions where the steady-state flow patterns are disrupted, such as over the internal weld beads on the pipe body. In this case, the erosion or flow pattern near the region revealed the phenomenon of vortices flow, which primarily contributed to erosion corrosion and led to PWC of the weld bead at the same time. Impingement on the weld bead occurred as a result of fluid ejection due to the formation of flow vortices. Previously, Nøkleberg and Sønrtvedt [6] stated that cavitation occurs in chokes for multiphase flow if the local pressure is lower than the water vapour pressure. Due to moisture and gas flow, the hydrocarbon gas bubbles produced in the choke inlet collapse, resulting in cavitation formation. The presence of a high flow rate could also lead to high shear stress that could reduce the stability of the film of the inhibitor. According to [29], the existence of an inhibitor improved the galvanic impact of a weld and other regions. Serious localised corrosion of the welded metal can easily occur, in particular erosion

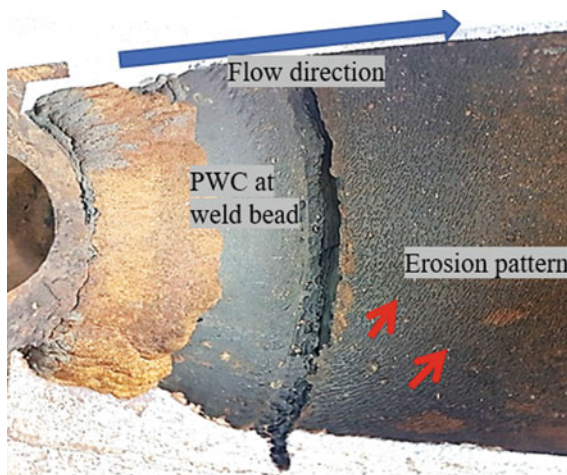


Fig. 7 Localized damage including erosion corrosion and preferential weld corrosion (PWC)

and galvanic corrosion at high flow rates and with a reducing of the efficiency of the inhibitor. Thus, even under inhibited conditions, the presence of fine debris from the corrosion product in the internal choke, especially at the weldment area, induces erosion and preferential weld corrosion. The instability of the inhibitor film at the weldment, especially near the eroded area, and its electrochemical negativity cause the weldment to be selectively disrupted compared to the other region.

3.7 Preferential Weld Corrosion (PWC)

Also displayed in Fig. 7 is the preferential weldment corrosion which contributed to the leakage. It is demonstrated that the leak of the pipeline should be attributed to the galvanic corrosion or preferential weld corrosion induced by less corrosion resistance and electronegativity of weldment compared to the inlet and outlet region [15, 19]. In this operation, nickel filler type ER7018 was employed for the welding of choke body. According to [19], a variation of regions of weldment possesses a different electrochemical potential value that contributed to a variation of susceptibility to corrosion. The weldment is anodic to the parent metal, then the localized metal loss can be easier to take place in this region.

The composition of the region, as tabulated in Table 1, confirmed that the chromium weight percent at weldment is 0.0926 wt.%, which is less than 5 and 12 times the composition of the chromium at the inlet and outlet regions, respectively. As a result of the lower chromium content, the weldment has lower corrosion resistance than regions with higher chromium content. Any high chromium content region is expected to have galvanic resistance due to the significant effect of chromium content. Furthermore, the formation of Cr-rich compounds in the corrosion product, i.e. FeCO_3 , also offers corrosion resistance. The more chromium in the alloy, the greater the amount of chromium compounds that form the protective layer [30]. However, in this situation, the impact of flow vortices aggravates corrosion at the weldment. This effect is exacerbated further by the limited surface areas of the weldment (anode) in comparison to the large surface area of the parent content (cathode). The increased hardenability of alloyed steel caused by coarsening of Cr-rich carbide precipitates often increases localised corrosion caused by microstructure transformation [19].

3.8 A Synergy of Erosion-Preferential Weld Corrosion (PWC) Effect

From the damage analysis, it can be found that the extensive metal loss was located right beside the choke seat location that possibly where the initiation of the gas vortex. This position also exhibited a reduction in wall geometry, which contributed

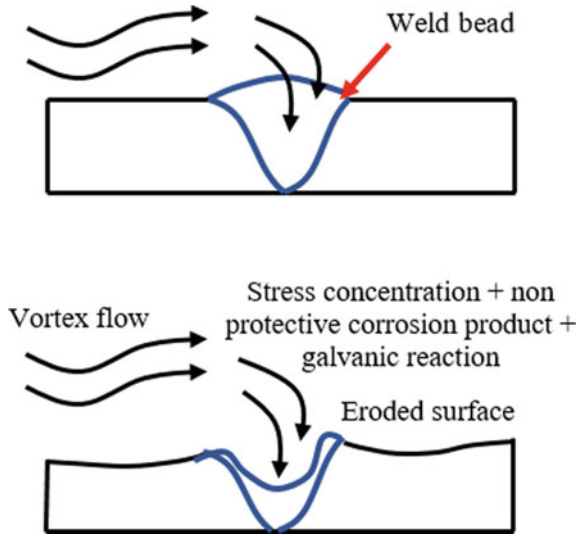


Fig. 8 The impact of stress concentration, non-protective corrosion product and galvanic reaction on the PWC

to the gas vortex. The droplets and particles in the vortices flow leading to alloy's film thinning that can weaken the corrosion resistance at the weldment. The geometric inhomogeneity near the welded joint can also lead to stress concentration at the weld bead [31]. High stress can affect corrosion by changing the properties of the corrosion product film and disrupts over the weld bead. Because of the action of the stresses, localised corrosion tends to occur at the weld bead, and the corrosion product film integrity and adhesion is lost. The corrosion product completely detached and offered no protection, as well as no resistance due to the lower chromium content. The impact of stress concentration, non-protective corrosion product and galvanic reaction on the PWC is illustrated in Fig. 8.

3.9 Analysis of Corrosion Product

The corrosion product is viewed in the brownish color, the common iron carbonate, FeCO_3 composition. The SEM micrograph of the corroded choke body with the accumulation of corrosion product is depicted in Fig. 9. As exhibited in the figure, the surface appeared to have tiny pits and loose corrosion products. Cracks can also be seen that were caused by surface dehydration.

A few EDX analysis was carried out to reveal the chemical compositions of the corrosion product. Figure 9 showed one of the SEM-EDX spectrum 1 result. The corrosion product mainly contained the elements of C, Al, Si, S, Cr, Mn, Fe and Ni. The elements of Si, Cr, Mn, Fe and Ni were from the metal-based elements.

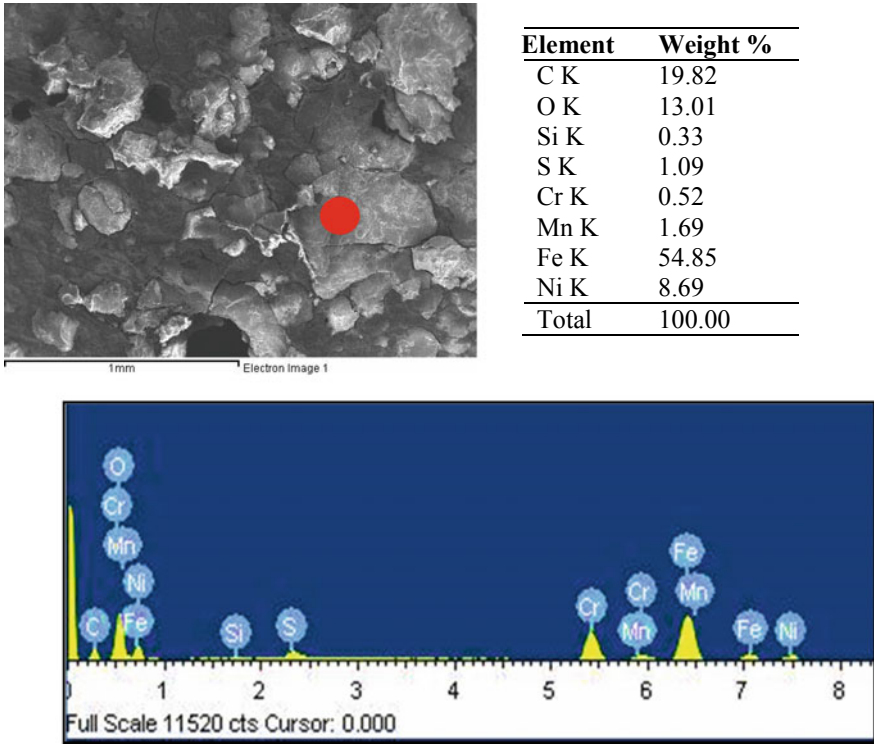


Fig. 9 SEM micrograph and EDX spectrum of the corroded choke body with accumulation of corrosion product consists of iron carbonate, FeCO₃

Carbon, C and oxide, O elements were also considered as the corrosive elements, with the high composition (%) was found. The corrosion product on the alloy was also analyzed with XRD spectra as provided in Fig. 10. The peak was found match with the composition of FeCO₃. Detection of some compounds such as FeS seems limited, probably due to less presence of H₂S. Also, there must be some compounds, such as Fe₂O₃ compounds, which were undetected by XRD.

Two phase chemical reactions that involve in the formation of corrosion product are provided in the reaction (1)–(6) [3]. The iron carbonate, FeCO₃ are the main corrosion products of carbon steel typically formed in the reaction involved with CO₂ corrosion. The medium in operation is also containing wet gas of H₂S that reacted with CO₂. CO₂ then is dissolved in the medium and formed weak H₂CO₃ acid resulting in an acidic and corrosive solution that ingresses damage of carbon steel. The reaction scheme is shown in the following (1)–(4) reactions.



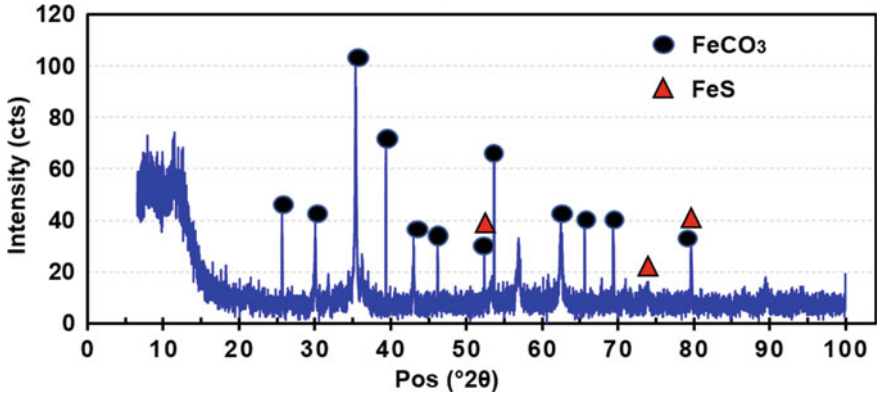
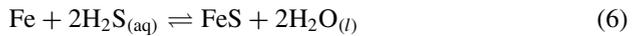
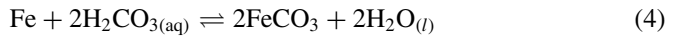


Fig. 10 XRD analysis indicating FeCO₃ as the main corrosion product. Low peak intensities dedicated to FeS, due to the presence of H₂S



Besides, FeS is also formed as a corrosion product from the second phase reaction of carbon steel with the H₂S from the following chemical reactions (5) and (6). However, less intensity of FeS peak is presented in XRD analysis, due to the little percentage of H₂S composition in the medium. Corrosion products are generally protective or corrosive depending on pH and ambient temperature. The morphology and composition of the corrosion product decide whether an attack manifests itself as worst-case corrosion, low corrosion with protective films, or mesa corrosion. The corrosion layer also affects the efficiency and availability of the corrosion inhibitor at the surface and thus play an important role for the inhibitor. When the FeCO₃ product is formed at a high temperature, normally greater than 60 °C, the formation rate is rapid and the supersaturation is low. Dense crystalline films that offer good protection often are created. While, with the low temperature of the medium, the relative supersaturation of FeCO₃ product formation is high. The corrosion product exhibited low crystallinity, porous, loosely adherent, and much less protective than those formed at higher temperatures [32].

4 Conclusions

Throughout this analysis, the following points could be drawn:

- (1) The dominant cause of leakage in the choke valve is preferential weld corrosion (PWC) at the weld bead in the CO₂ medium.
- (2) PWC is exacerbated by the action of the stresses and the formation of non-protective corrosion product film. The flow pattern associated with the erosion corrosion was evidenced due to the turbulence/vortex flow that induces stress within the weldment.
- (3) The coarsening of chromium carbide precipitates increases the hardness value at weldment.
- (4) The driving force for the PWC is less chromium composition of the weldment region that decreases the corrosion resistance of the weldment. It is also associated with the galvanic effect from the difference between the areas of the weldment and the inlet and outlet. The weldment region acts as the anode with the small area as compared to the large area of the parent material that served as the cathode.

Acknowledgements The authors would like to thank the Ministry of Higher Education for providing financial support under Fundamental Research Grant Scheme (FRGS) No. FRGS/1/2019/TK05/UMP/02/5 (University reference RDU1901128) and Universiti Malaysia Pahang for laboratory facilities.

References

1. Dawson JL, John G, Oliver K (2010) Management of corrosion in the oil and gas industry. Shreir's Corros 3230–3269
2. Moiseeva LS (2005) Carbon dioxide corrosion of oil and gas field equipment. Prot Met
3. Kahyarian A, Achour M, Nesic S (2017) CO₂ corrosion of mild steel. Elsevier Ltd
4. Di Schino A (2019) Environmental impact of steel industry. Handbook of environmental materials management, pp 2463–2483
5. Pyshmintsev YI, Veselov IN, Maltseva AN, Uskov DP (2018) Specific effects of microalloying elements on the development of the strength properties of low-alloyed chromium-molybdenum pipe steels. AIP Conf Proc 2053
6. Nøkleberg L, Søntvedt T (1995) Erosion in choke valves-oil and gas industry applications. Wear 186–187:401–412
7. Oil AFOR (2019) Method and apparatus for oil and gas operations, p 1
8. Liu W, Shi T, Li S, Lu Q, Zhang Z, Feng S, Ming C, Wu K (2019) Failure analysis of a fracture tubing used in the formate annulus protection fluid. Eng Fail Anal 95:248–262
9. Rintamäki K, Kuusela P (2010) Stress corrosion cracking of carbon steel in amine units. Key Eng Mater 2177–2184
10. Tawancy HM, Alhems LM (2016) Damage analysis of choke bean used in an oil–gas well. Case Stud Eng Fail Anal 7:56–64
11. Liu Z, Gao X, Du L, Li J, Li P, Yu C, Misra RDK, Wang Y (2017) Comparison of corrosion behaviour of low-alloy pipeline steel exposed to H₂S/CO₂-saturated brine and vapour-saturated H₂S/CO₂ environments. Electrochim Acta 232:528–541

12. das Chagas Almeida T, Bandeira MCE, Moreira RM, Mattos OR (2017) New insights on the role of CO₂ in the mechanism of carbon steel corrosion. *Corros Sci* 120:239–250
13. Song FM (2010) A comprehensive model for predicting CO₂ corrosion rate in oil and gas production and transportation systems. *Electrochim Acta* 55:689–700
14. Darihaki F, Hajidavalloo E, Ghasemzadeh A, Safian GA (2017) Erosion prediction for slurry flow in choke geometry. *Wear* 372–373
15. Adegbite MA, Robinson MJ, Impey SA (2016) Evaluation of flow enhanced preferential weld corrosion of X65 pipeline steel using a novel submerged impingement jet, pp 1–12
16. Barker R, Hu X, Neville A (2013) The influence of high shear and sand impingement on preferential weld corrosion of carbon steel pipework in CO₂-saturated environments. *Tribol Int* 68:17–25
17. Zhu J, Xu L, Feng Z, Frankel GS, Lu M, Chang W (2016) Galvanic corrosion of a welded joint in 3Cr low alloy pipeline steel. *Corros Sci* 111:391–403
18. Bland LG, Troconis BCR, Santucci RJ, Fitz-Gerald JM, Scully JR (2016) Metallurgical and electrochemical characterization of the corrosion of a Mg-Al-Zn alloy AZ31B-H24 tungsten inert gas weld: galvanic corrosion between weld zones. *Corrosion* 72:1226–1242
19. Pantelis DI, Tsiourva TE (2017) Corrosion of weldments. Elsevier Ltd
20. ASTM International (2015) Standard specification for steel castings suitable for pressure service
21. Bignozzi MC, Calcinelli L, Carati M, Ceschini L, Chiavari C, Masi G, Morri A (2019) Effect of heat treatment conditions on retained austenite and corrosion resistance of the X190CrVMo20-4-1 stainless steel. *Met Mater Int*
22. Hao L, Ji X, Zhang G, Zhao W, Sun M, Peng Y (2020) Carbide precipitation behavior and mechanical properties of micro-alloyed medium Mn steel. *J Mater Sci Technol* 47:122–130
23. International N (2015) Methods and controls to prevent in-service environmental cracking of carbon steel weldments in corrosive petroleum refining environments, p 36
24. Escrivà-Cerdán C, Ooi SW, Joshi GR, Morana R, Bhadeshia HKDH, Akid R (2019) Effect of tempering heat treatment on the CO₂ corrosion resistance of quench-hardened Cr-Mo low-alloy steels for oil and gas applications. *Corros Sci*
25. Ju Y, Goodall A, Strangwood M, Davis C (2018) Characterisation of precipitation and carbide coarsening in low carbon low alloy Q&T steels during the early stages of tempering. *Mater Sci Eng A*
26. Miller MK (1998) Carbide precipitation in martensite during the early stages of tempering Cr- and Mo-containing low alloy steels. *Acta Mater*
27. Dai T, Lippold JC (2018) Tempering effect on the fusion boundary region of alloy 625 weld overlay on 8630 steel. *Weld World*
28. Saha DC, Nayak SS, Biro E, Gerlich AP, Zhou Y (2014) Mechanism of secondary hardening in rapid tempering of dual-phase steel. *Metall Mater Trans A* 45:6153–6162
29. Alawadhi K, Robinson MJ (2011) Preferential weld corrosion of X65 pipeline steel in flowing brines containing carbon dioxide. *Corros Eng Sci Technol* 46:318–329
30. Sun J, Sun C, Lin X, Cheng X, Liu H (2016) Effect of chromium on corrosion behavior of P110 steels in CO₂-H₂S environment with high pressure and high temperature. *Materials* 9:1–14
31. Qiao Q, Cheng G, Wu W, Li Y, Huang H, Wei Z (2016) Failure analysis of corrosion at an inhomogeneous welded joint in a natural gas gathering pipeline considering the combined action of multiple factors. *Eng Fail Anal* 126–143
32. Dugstad A (2006) Fundamental aspects of CO₂ metal loss corrosion. Part I: Mechanism. In: *Corrosion Nace expo 2006*, pp 1–18